The Astrophysical Journal, 936:49 (9pp), 2022 September 1 https://doi.org/10.3847/1538-4357/ac85e3

Solar and Stellar Flares: Frequency, Active Regions, and Stellar Dynamo

M. M. Katsova[1], V. N. Obridko[2,3], D. D. Sokoloff[4,2,5], and I. M. Livshits[1,6]
[1] Sternberg State Astronomical Institute, M.V. Lomonosov Moscow State University, Universitetskij prosp. 13, 119991, Moscow, Russia; ilyaliv@bgu.ac.il
[2] IZMIRAN, 4 Kaluzhskoe Shosse, Troitsk, Moscow, 142190, Russia
[3] Central Astronomical Observatory of the Russian Academy of Sciences at Pulkovo, St. Petersburg, Russia
[4] Moscow State University, Moscow, 119991, Russia
[5] Moscow Center of Fundamental and Applied Mathematics, Moscow, 119991, Russia
[6] Department of Geography and Environmental Development, Ben-Gurion University of the Negev, P.O.B. 653, 84105, Beer-Sheva, Israel
Received 2022 March 12; revised 2022 July 18; accepted 2022 July 31; published 2022 August 30

Abstract

We demonstrate that for weak flares the dependence of their frequency occurrence on spottedness can be rather weak. The fact is that such flares can occur in both small and large active regions. At the same time, powerful large flares of classes M and X occur much more often in large active regions. In energy estimates, the mean magnetic field in starspots can also be assumed to be equal to the mean field in the sunspot umbra. So the effective mean magnetic field is 900 Mx cm^{-2} in sunspots and 2000 Mx cm^{-2} in starspots. Moreover, the height of the energy storage cannot be strictly proportional to $A^{1/2}$. For stars, the fitting factor is an order of magnitude smaller. The analysis of the occurrence rate of powerful solar X-ray flares of class M and X and superflares on stars shows that, with allowance for the difference in the spottedness and compactness of active regions, both sets can be described by a single model. Thus, the problem of superflares on stars and their absence on the Sun is reduced to the problem of the difference in the effectiveness of the dynamo mechanisms.

Unified Astronomy Thesaurus concepts: Solar activity (1475); Stellar activity (1580); Solar flares (1496)

1. Introduction

Solar flares are a spectacular phenomenon in the solar magnetic activity. They can more or less directly affect the Earth, and the study of solar flares is of both applied and academic interest. The origin of solar flares is obviously associated with the solar magnetic field, and in this sense, it is related to the action of the solar dynamo responsible for the formation of the magnetic field. The study of solar flares, which can be considered a traditional part of solar physics, has made impressive progress (among many others, see, e.g., Parker 1963; Priest & Forbes 2002; Benz 2008; Benz & Güdel 2010; Kretzschmar 2011; Emslie et al. 2012; Schrijver et al. 2012; Somov 2013; Aschwanden et al. 2014).

Of course, phenomena similar to the solar flares and known as stellar flares occur on various stars. As is known, the total energies of solar flares vary in a wide range of 10^{24}–10^{32} erg from the weakest events to the strongest ones (see, e.g., Zimovets et al. 2020). Stellar flares are best studied on low-mass, red dwarf stars, and their total energies exceed the maximum solar value by several orders of magnitude (see, e.g., Herbst et al. 2021, and references therein). Besides, the most powerful of these flare phenomena were mainly recorded on very young dwarfs, including T Tau stars, members of open clusters, and fast-rotating subgiants and giants, as well as on chromospherically active components of RS CVn−type close binaries (see, e.g., García-Alvarez et al. 2003; Fernández et al. 2004; Schmitt et al. 2019).

It is known that the most powerful flares on the Sun are rare phenomena that are characterized by a sudden rise in optical continuum emission, and they are called white-light flares. Since a source of the flare optical continuum emission has a low contrast against the photosphere, has a small flare area, and lives a short time (a few minutes), this prevents us from revealing the temporal profile of the flare radiation. Nevertheless, powerful Sun-as-a-star flares were detected in long-term data on total solar irradiance (TSI; Kretzschmar 2011). Note that the same problems make the detection of optical flares on single main-sequence G stars difficult, so it was thought that white-light flares have not been seen there until the Kepler mission. Only recently does definite information appear about the flare activity of these stars (Jackman et al. 2018; Bondar' et al. 2021; Katsova et al. 2021). From the other side, Kashapova et al. (2021) showed that time profiles of solar flares in the UV continuum emission are similar to impulsive flare light curves registered on the red dwarf during the Kepler mission. This result supports the point that the existence of optic flares in G stars can be suspected in the UV data. Indeed, they were found recently in GALEX near-UV data for these stars (Brasseur et al. 2019).

It seems natural to use the ideas gained from the study of solar flares to understand stellar flares as similar phenomena in the stellar physics. However, as shown by the progress in observations of the stellar activity, stars reasonably similar to the Sun can produce flares substantially more energetic than the strongest solar ones.

The total energies of the strongest stellar flares can exceed 10^{36} erg in the optical wavelength range (see, e.g., Herbst et al. 2021). As for the flare activity of the solar-type main-sequence G stars, there was very little information prior to the Kepler mission (e.g., Jackman et al. 2018; Bondar' et al. 2021; Koller et al. 2021). The superflare concept applicable to powerful nonstationary stellar phenomena was introduced when the first results of the Kepler mission, which operated in 2009–2018 and detected huge flares on G-type stars, were published (Maehara et al. 2012; Shibayama et al. 2013; Maehara et al. 2015; Namekata et al. 2019; Okamoto et al. 2021a). These

publications reported the detection of major stellar flares on solar-type stars with total energies from 10^{33} to 10^{37} erg at optical wavelengths. A more detailed analysis showed that most flares had a total energy of 10^{33}–10^{34} erg (Tu et al. 2021), while only a small fraction of the phenomena could be considered superflares with energies $E = 10^{35}$–10^{36} erg. Now, it is clear that the most powerful events with $E > 10^{36}$ erg occur on components of the close binary stellar systems, on subgiants and giants, or on very young and/or fast-rotating stars that have not reached the main sequence (Balona 2015; Katsova & Nizamov 2018; Tu et al. 2021). The results of analysis of numerous multiwavelength observations of stellar flares and other nonsteady phenomena on red dwarfs and solar-like stars reviewed by Gershberg (2005) provide evidence for their common physical nature with solar flares and confirm this idea first expressed by Gershberg & Pikel'ner (1972). The process can be approximately described as a deposit of the free energy of the nonpotential magnetic field in a certain volume, its impulsive release during nonsteady event, and the subsequent response of the atmosphere to the resulting acceleration of particles and plasma heating. At the same time, already Gershberg et al. (1987) paid attention to the deficiency of up-to-date models of solar flares for an explanation of the strongest stellar flares. In particular, it seems plausible that dynamo underlying magnetic field evolution in superflares stars is not fully identical to the conventional solar dynamo.

Indeed, the maximum total flare energy on solar-type stars can be several times more than (3–5) $\times$ 10^{34} erg. This estimate is based on the magnetic virial theorem (Katsova & Livshits 2015; Livshits et al. 2015). A similar value is discussed now in the recent statistics of all the primary Kepler mission data (Okamoto et al. 2021a).

It looks plausible that magnetic configurations sufficient to accumulate corresponding magnetic energy have to be different in size and/or morphology from conventional sunspots.

Nevertheless, we believe that the problem of superflares is, perhaps, less dramatic than it seemed earlier; however, it still does exist and is in need of explanation. We are going to propose a corresponding revision in this paper.

To assess the similarity or difference between the solar and stellar flares correctly, it is necessary to take into account a number of circumstances.

First, a double selection of observational data must be taken into account. For natural reasons (the sensitivity of the equipment), only the most powerful white-light flares, which are extremely rare in the Sun (about 0.4% of the total number of flares observed on the Sun over 15 yr; see Section 2), are recorded on stars. In addition, the rotational modulation technique makes it possible to detect only the largest concentrated spots or spot groups on stars. We discuss these issues in Sections 1 and 2.

Another circumstance that must be taken into account is that flares of different energy depend in different ways on the area of the active region. The frequency and energy of weak X-ray flares B and C are virtually independent of the area of the active region and therefore cannot be used to assess the similarity or dissimilarity with superflares on stars. This issue is discussed in Section 2.

And finally, when evaluating the total magnetic energy in the active region, we cannot use the extreme values of several kG, which are observed in sunspots. These values correspond to a very small part of the spot. To find the total energy, it is necessary to obtain the integral values, for which we have to know the distribution of the magnetic field over the active region. In this case, we cannot use the photometric values of the spot area but have to introduce the concept of a magnetic boundary and, additionally, to determine the relative fraction of the umbral area. These estimates are given in Section 3.

These problems were discussed by various authors (see, e.g., Benz 2008; Benz & Güdel 2010). A particularly detailed and thorough analysis was carried out by Berdyugina (2005), who not only described methods for studying starspots but also provided extensive observational material, which was subsequently used by other authors (Aulanier et al. 2013; Notsu et al. 2013; Shibayama et al. 2013; Maehara et al. 2015; Namekata et al. 2019; Herbst et al. 2021; Okamoto et al. 2021a). It should be noted that the procedures used to determine the spot areas on the Sun and stars are essentially different. In the former case, the observer directly calculates the area of each spot from the full image of the Sun and then sums up the values obtained. The penumbra is traditionally included in the spot area. The procedure of determining the total spottedness on stars is more complicated. First of all, one has to find out the variation in the star brightness. The methods for determining this variation, such as the light-curve modeling, Doppler imaging, Zeeman–Doppler imaging, and molecular band modeling, are described in detail by Berdyugina (2005). These methods are based on the use of different radiation characteristics of a star, continuous spectrum in different ranges, different spectral lines, Doppler effect, magnetic splitting, and molecular spectrum. Generally speaking, these data can refer to different layers in the stellar atmosphere. Standing apart is the spot temperature. The large sunspot areas and temperature contrasts found in active stars suggest that the photometric and spectroscopic variability of these stars is dominated by the starspot umbra. Our current knowledge about starspot temperatures is based on measurements obtained from simultaneous modeling of brightness and color variations, Doppler imaging, modeling of molecular bands, and atomic line depth ratios, the latter being the most accurate method. A representative sample of starspot temperatures for active dwarfs, giants, and subgiants is provided in Table 5 and plotted in Figure 7 in Berdyugina (2005).

Then, the spot area ($A_{\rm spot}$) of superflare stars is estimated from the normalized amplitude of light variations ($\Delta F/F$) by using the following equation:

$$A_{\rm spot} = \frac{\Delta F}{F} A_{\rm star} \left[1 - \left(\frac{T_{\rm spot}}{T_{\rm star}} \right)^4 \right]^{-1}, \quad (1)$$

where $A_{\rm star}$ is the apparent area of the star and $T_{\rm spot}$ and $T_{\rm star}$ are the temperature values of the starspot and stellar photosphere, respectively.

No matter how the temperature values are obtained, it turns out that in solar-like stars they are close to the temperature in the sunspot umbra (see Berdyugina 2005, Table 5). This means that, in fact, we find the total area of the umbra, or, to be more precise, the starspot area on stars can be considered to be coinciding with the area of the umbra. Therefore, in energy estimates, the mean magnetic field in starspots can also be assumed to be equal to the mean field in the sunspot umbra.

Considering all of the abovementioned circumstances, we arrived at a conclusion that the problem of superflares on stars and their absence on the Sun is reduced to the difference in the effectiveness of the dynamo mechanism. This conclusion and certain consequences for the problem of the generation of magnetic fields in the Sun and stars are discussed in Section 4.

2. Comparing Solar and Stellar Flares

The structure of our research depends substantially on the particular difficulties of comparing the solar and stellar flares listed in this section.

First of all, we have to emphasize that the task of comparing the stellar and solar flares is far from straightforward. Indeed, it is often stated that (see, e.g., Herbst et al. 2021) solar flares do not fit into the linear trend visible in stellar data. The point, however, is that due to the instrumental limitations, the stellar flares are only white-light flares, which are the most energetic ones, while the weak flares are not observable and therefore are absent on the plot. In contrast, the solar data contain all flares with peak X-ray flux from 10^{-7} W m^{-2} up to the flux of the order of 10^{-3} W m^{-2}, i.e., from subflares up to the major proton events. The most energetic flares belong to classes M and X. This makes up the energy range from 10^{28} to 10^{32} erg and corresponds to a spottedness of no more than 3000 m.v.h. The minimum detectable spottedness on stars is approximately 1000 m.v.h. (Okamoto et al. 2021a, 2021b), but in general stellar flares have energies from 10^{34} to 10^{36} erg, which corresponds to the spottedness range from 0.01 to 0.3 of the area of the visual solar hemisphere.

Another relevant problem is connected with the fact that the total spot area (spottedness) is not the only parameter that determines directly the flare energy. This point is discussed in Section 3.

Note also that the expression "spot area" or "spottedness" is understood quite differently when referred to the Sun and stars. As for the Sun, we assume that the spottedness is just the total area of individual spots visible in the white light relative to the area of the solar hemisphere. In contrast, the stellar spottedness is usually estimated from the rotation modulation of the stellar brightness without taking into account the spot distribution over the star surface. This method, however, gives basically different estimates for a single large spot and for many spots of moderate size distributed more or less homogeneously over the stellar surface. In particular, when observing the Sun as a star by this method, we see almost no rotational modulation even in the periods of very high activity.

Summarizing all of the above, we expect a strong selective effect in stellar observations, which gives preference to the contribution of a single or a few very large spots. Therefore, the solar data have to be properly selected to be comparable to the stellar ones.

It can be expected that for weak flares the dependence on spottedness can be rather weak. The fact is that such flares can occur in both small and large active regions. At the same time, powerful large flares of classes M and X (the peak flux larger than 10^{-5} W m^{-2}) occur much more often in large active regions. It is known that there are positive correlations between the sunspot coverage and the energy of the largest solar flares (see, e.g., Sammis et al. 2000).

To test these considerations, we performed an additional analysis. The occurrence rates N of flares of different classes were estimated for the period 1992–2016 using data from the catalog http://hec.helio-vo.eu/hec/hec_gui.php, which contains 44,566 X-ray flares. The GOES Soft X-ray Flare List was used. The flare classes are determined by their peak fluxes as follows: B stands for fluxes $(1–9)\times 10^{-7}$ W m^{-2} (17,747 flares), C stands for $(1–9)\times 10^{-6}$ W m^{-2} (24,190 flares), M corresponds to $(1–9)\times 10^{-5}$ W m^{-2} (2449 flares), and X stands for $(1–9)\times 10^{-4}$ W m^{-2} (180 flares). Based on these data, we calculated the monthly mean occurrence rates of flares of each class and compared them with the monthly spottedness data taken from https://solarscience.msfc.nasa.gov/greenwch/sunspot_area.txt. Then, we gathered separately the data for classes B and C and the data for classes M and X and plotted them versus the spottedness (Figure 1). For weak flares (B and C), the occurrence rate $N_{\rm BC}$ is almost independent of spottedness (Figure 1). The exponent is only 0.237, with a correlation coefficient of 0.514:

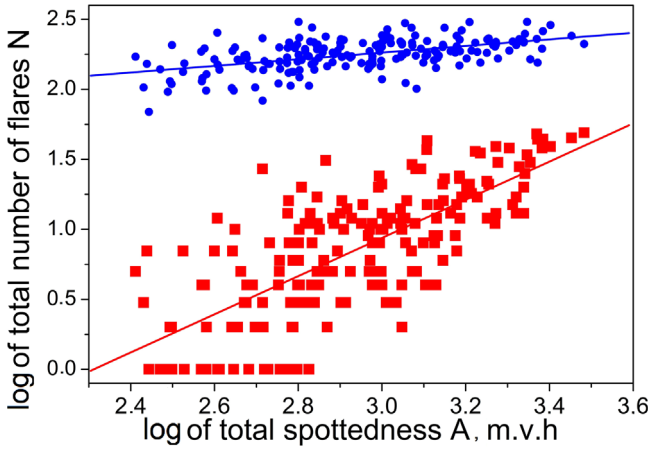

Figure 1. Monthly mean occurrence rates of flares N vs. monthly mean spottedness A (top, blue circles—B- and C-class flares; bottom, red squares—M- and X-class flares). The colored lines show the result of a linear regression of each of the two samples of flares.

$$\log N_{\rm BC} = 1.55185 \pm 0.0845 + (0.23674 \pm 0.0286)\log A. \quad (2)$$

A pronounced relationship between the occurrence $N_{\rm MX}$ and the spottedness A is seen only for strong flares of class M and X (Figure 1, bottom). The exponent of the power-law dependence for these flares is much higher and amounts to 1.363, with a correlation coefficient of 0.728:

$$\log N_{\rm MX} = -3.152 \pm 0.2749 + (1.36349 \pm 0.09318)\log A. \quad (3)$$

An important characteristic of flares is their occurrence rate. The simplest and most physically meaningful relationship between the flare energy and occurrence rate is expressed by a power function. Figure 2, based on the picture from Gershberg et al. (1987) and repeated later by Gershberg (2005), shows the relationship between the energy of flares observed in the photometric B band (E_B) and their occurrence rates for different dwarf stars, indicated on the plot, and for the stars of Pleiades and Orion as well. These data are the result of thousands of hours of photoelectric monitoring observations at various world observatories. By now, more than 3000 stars of the type under discussion have been registered. The data shown in the figure refer mainly to red dwarfs (spectral class M). The total energy ranges from 10^{28} to 10^{36} erg, which is much broader than the superflare range (10^{33}–10^{36} erg). The energy range of superflares was determined from observations of the Kepler mission, which could not discriminate weak flares because of the background noise. More recent data obtained with the Transiting Exoplanet Survey Satellite (TESS) and Large Sky Area Multi-Object Fiber Spectroscopic Telescope (LAMOST) are described by Tu et al. (2021). The authors developed their own technique, which allowed recording weaker events than those detected by Kepler. Colombo et al. (2022) validated the

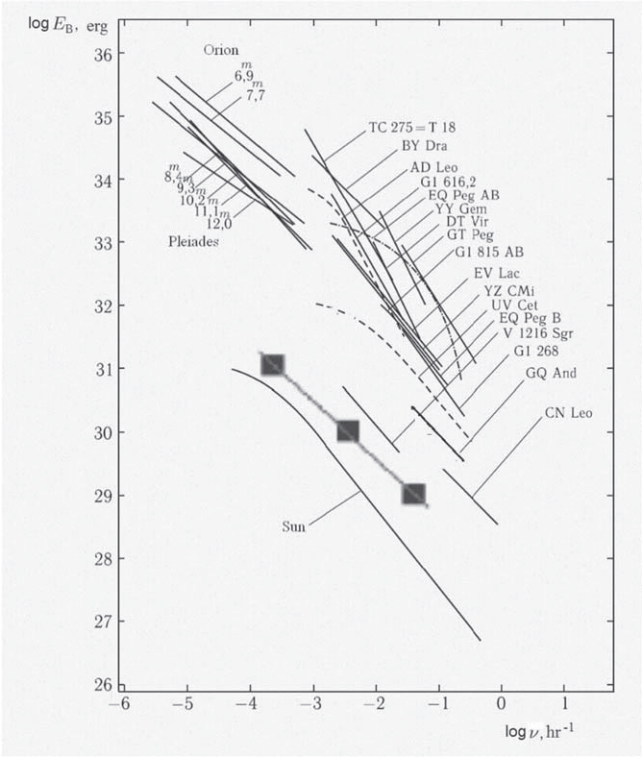

Figure 2. The energy of flares in connection with their occurrence rates on different stars. The curve for the Sun is based on Hα data; the squares and thick line are plotted according to X-ray data.

procedure by comparing the results obtained with other techniques by Martiol et al. (2021) for AU Mic and found a rate of events of ≈5 flares day^{-1} with energy $E_f > 5 \times 10^{31}$ erg. In addition to that, they studied the system DS Tuc A and found a rate of energetic events of ≈2 flares day^{-1} with energy greater than 2×10^{32} erg. It is interesting to note that these data agree well with ground-based observations of red dwarfs (see Figure 2).

It should be noted that a good agreement between the observed relation and the power function, which is represented by a straight line in the logarithmic diagram, does not exist in the entire energy range. Sometimes there is saturation for very strong flares and a sudden dip due to the observational selection for very weak flares (Gershberg 2005). Therefore, in general, the figure shows only the linear sections of the relation. Significant deviations from linearity are observed for UV Ceti, AD Leo, and EQ Peg AB and are shown by dotted lines. Additionally, the figure shows the relationship for solar flares in Hα. The total length of the dynamic energy range of flares on each star does not exceed two orders of magnitude.

The range of the energies and occurrence rates on the diagram is rather broad (7–9 orders of magnitude), while the angular coefficients of the dependencies $\beta = d \log \nu / d \log E$ lie in a narrow range from −0.5 to −0.9. In the clusters, they are somewhat larger in the absolute value (from −0.8 to −1.0); for solar flares in Hα, $\beta = -0.8$ (Gershberg 2005). We have plotted a similar curve using observations of X-ray flares mentioned above. The occurrence rates are 0.110 hr^{-1} for class C flares (24190 events), 0.0112 events hr^{-1} for class M flares (2449 events), and 8.208×10^{-4} hr^{-1} for class X flares (180 events). The dip for class B flares was ignored as it was when plotting the relations for star flares. The result is represented in Figure 2 by a thick line and large squares. One can see that, here, the value of β (−1.06) is close to the values for superflares in the clusters and is typical of stars of approximately the solar age (Gershberg 2005). The similarity of the values of β shows that despite the significant difference in energy, superflares on stars and solar flares are apparently determined by the same processes (Gershberg 2005).

It should be noted that on the Sun the linear part of the dynamic energy range also does not apparently exceed 2–3 orders of magnitude. If there were no saturation, and with the observed value of β, at least one superflare with an energy in the range of 10^{34}–10^{35} erg would have to occur on the Sun every 550 yr, which is not confirmed by the historical and archaeological data available.

Note also that, as follows from Figure 2, flares of the same energy on the Sun (and apparently in general on G dwarfs) are 30–100 times less frequent than on red dwarfs.

To avoid misunderstandings, we note that the value of ν used by us, calculated per 1 hr, corresponds to the f_* used by Tu et al. (2021), which is calculated per 1 yr, but does not coincide with the index f_n introduced there, in which additional normalization is carried out for the number of observed stars and the energy range. This more physically sound parameter yields $\beta = -1.76$.

3. Scaling Stellar Data

Now, our task is to suggest a reasonable scaling for the energy E of stellar flares. We depart from the conventional assumption that the energy is determined by the magnetic energy density $B^2/8\pi$ (where B is the magnetic field) and the volume of energy accumulation. The latter is proportional to the spot area A and the height h of the volume.

We depart from the viewpoint that the initial flare energy release originates in the magnetic energy in a volume. This energy is converted into particle acceleration, optical and X-ray radiation, and plasma motions (Emslie et al. 2004; Belov et al. 2005; Vilmer 2012). The immediate origin for the energy release in a flare is a current dissipation that is proportional to the scaling factor f_r to the total magnetic field energy. Estimates of f_r contain various uncertainties (Schrijver et al. 2012) and vary from 0.01 to 0.5. We argue that solar and stellar flares are physically similar, and fortunately we can accept that f_r is the same for solar and stellar flares. Giving below corresponding references, we do not focus our attention on this scaling factor.

Thus, the total energy released in a flare is described by the expression

$$E = f_r \int \frac{B^2}{8\pi} dV. \quad (4)$$

Direct calculations by this formula are difficult even for the Sun and require observations with good spatial resolution and high-quality full-vector maps of the magnetic field. Such calculations with some additional assumptions have been performed by several authors (see, e.g., Livshits et al. 2015; Zimovets et al. 2020) and generally confirmed the above concept with the parameter $f_r \approx 0.1$. However, such calculations are completely impossible today for stars, and therefore a simpler formula is used:

$$E = f_r \frac{\overline{B^2}}{8\pi} V. \quad (5)$$

Here B is the mean field in the given volume, which is determined as follows:

$$V = \overline{A} \cdot \overline{H}. \quad (6)$$

The situation with other scaling factors f_h and f_s is more delicate, as they may be substantially different for the Sun and stars. The point is that by estimating B we can use magnetic field averaged over the whole sunspot, while for the stars we have to use magnetic field averaged over the umbra, as magnetic field in the whole starspot is not accessible for observations. The total sunspot area A for the Sun is determined photometrically and includes sunspot umbra and penumbra. As for stars, the value A is determined using Equation (1) based on spectral temperature related to the umbra (Berdyugina 2005; Herbst et al. 2021). We need the scaling factor f_s to reproduce this difference:

$$\overline{A} = f_s A_{\rm spot}. \quad (7)$$

The value of $\overline{B}$ changes accordingly. For the Sun, we have to use the mean field value over the entire sunspot, and for the stars, we have to use the mean field in the spot umbra.

And finally, to estimate $\overline{H}$, we use the expression connecting the height of the energy release region to the radius of a round spot:

$$H = f_h A_{\rm spot}^{1/2}. \quad (8)$$

Note that this approximation raises serious doubt. Here we also need to introduce a model parameter f_h, since the region of primary energy release must contain free (nonpotential) energy. Deviations from potentiality arise when the pressure and energy of plasma motions are greater than or comparable to the potential energy of the magnetic field. In the majority of solar flare models, the height H is 10,000–20,000 km, i.e., is comparable to the radius of a very large sunspot, but is much smaller than the radius of a stellar spot.

Without this additional parameter, very large values of A will yield too large H, e.g., at $A = 0.1$, we will get a height comparable to the radius of the star, which, obviously, cannot give any reasonable current density. This means that, at equal heights of the energy release region, the parameter f_h on the stars is smaller.

The other drawback of this approximation is that $\overline{H}$ is not an additive parameter. If several large spots are observed on the star, their area is summed up, and the parameter $\overline{A}$ increases proportionally, while the value of $\overline{H}$ does not change.

Combining these formulae, we obtain the following equation:

$$E = f_h \cdot f_s \cdot f_r (B^2/8\pi) A^{3/2}. \quad (9)$$

When comparing with observations, it is usually not taken into account that the magnetic field strength and the dimensionless fitting factors may change as the spot coverage changes (see, e.g., Maehara et al. 2012, 2015; Notsu et al. 2013; Okamoto et al. 2021a). Note that the above equation is nearly the same as Equation (9) in Notsu et al. (2013); however, we introduce scale factors, while Notsu et al. (2013) use observed quantities combined with a reasonable estimate of the ratio of the spot temperature to the stellar photospheric temperature. We use the scaling factors to take into account that solar and stellar data are obtained using substantially different methods.

Therefore, on the diagrams in logarithmic coordinates this dependence is represented as a straight line, and comparison with observations is carried out by selecting a constant value of the magnetic field. The usual conclusion is that it is not possible to find a constant field value at which Equation (9) would describe both solar and stellar flares. This does not take into account that both the B value and the fitting factors can be different on the Sun and stars.

As mentioned above in the Introduction, in sunspot observations the photometric picture is used to calculate the entire area of a sunspot including the penumbra. The sum of these values is defined as the spottedness and is contained in all solar catalogs. For stars, a different procedure is used, which is based on the temperature difference between the star and the observed spot. This difference corresponds to the temperature difference between the spot umbra and the star. This means that, in fact, we find the total area of the umbra, or, to be more precise, the area of a starspot can be considered to be coinciding with the area of the umbra. Therefore, in energy estimates, the mean magnetic field in starspots can also be assumed to be equal to the mean field in the sunspot umbra.

Thus, to estimate the parameters included in Equation (9), it is necessary to know the mean magnetic field in a spot. However, the sunspot boundaries are determined based on photometric properties. Unfortunately, there is still no generally accepted definition of the magnetic boundary of a spot. In this work, we used SDO/HMI observations to solve this problem.

We considered the daily SDO/HMI data on the line-of-sight magnetic field component for the period from 2010 May 1 to 2016 October 31—a total of 2375 days. The daily data on sunspot numbers were downloaded from the WDC-SILSO website, Royal Observatory of Belgium, Brussels (http://sidc.oma.be/silso/datafiles, version 2). The total daily sunspot areas were taken from the NASA website https://solarscience.msfc.nasa.gov/greenwch.shtml. The daily values of the line-of-sight field component were recalculated into the radial component by dividing by the cosine of the position angle. The area of each pixel was also corrected. Then, we calculated the relative fraction S_B of the area occupied by fields above a certain limit. This fraction was expressed in millionths of the solar hemisphere, as is customary when studying the total areas of sunspots.

These daily values are expressed in m.v.h. of the hemispheric area and are calculated for several thresholds ranging from 0 to 1800 G. As a first approximation to finding the magnetic field boundary, we calculated the regression between S_B and the total sunspot area. It turned out that, at the magnetic spot boundary of 550 G, the correlation between these values reaches 0.98. Moreover, this correlation is valid in a very narrow range; even at the threshold values of 500 and 575 G, the correspondence deteriorates.

The calculation procedure is described in more detail by Obridko & Shelting (2018). Close values for the magnitude of the vertical component of the magnetic field at the outer boundary of the penumbra are also given by Keppens & Martinez Pillet (1996), Solanki et al. (2006), Aulanier et al. (2013), and Borrero & Ichimoto (2011).

Assuming that the boundary of the spot area responsible for a flare corresponds to the magnetic field of 550 G, and plotting the mean magnetic field B_s in the spot versus the spottedness (Figure 3(a)), we learn that the spottedness $A = 300$ m.v.h. (i.e., 3×10^{-4} of the area of the visible solar hemisphere)

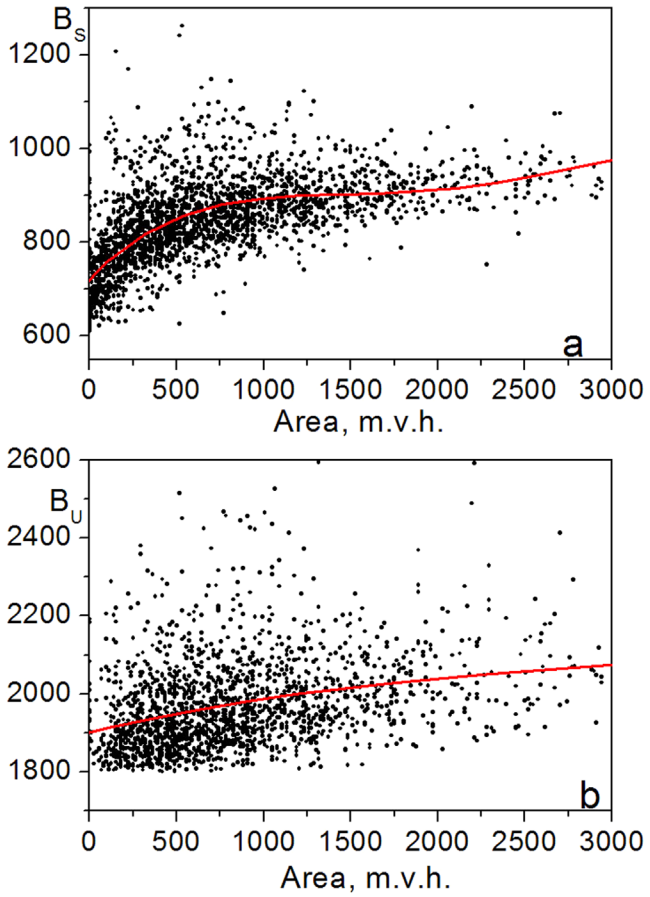

Figure 3. Mean magnetic field in the flaring sunspots (panel (a)) and starspots (panel (b)) vs. spottedness. The magnetic field is 550 G at the sunspot boundary and 1800 G in the starspot boundary.

corresponds to $B = 800$ G, while $A = 900$ m.v.h. gives $B = 900$ G. Taking into account that the area of the solar hemisphere is 3.044×10^{22} cm^2, we obtain from Equation (4) the following lower estimates for the total magnetic energies stored in sunspot regions with $A = 300$ m.v.h and $A = 900$ m.v.h.: $E = 8 \times 10^{32} f_h f_s f_r$ erg and $E = 5.8 \times 10^{33} f_h f_s f_r$ erg correspondingly.

When making similar calculations for stellar flares, we have to take into account that the spottedness $A = 3 \times 10^{-2}$ m.v.h. is rather high, and the starspot must be more compact than the sunspot to be distinguished by the rotation modulation of the stellar brightness.

As mentioned above, the method of determining the area from temperature data leads to the fact that the determined area of the spot is essentially the area of the umbra. Therefore, under the assumption that the average field in the umbra is the same in sunspots and starspots, it can be calculated based on the knowledge of the magnetic field at the umbra–penumbra boundary. Unfortunately, the method that was used above to determine the outer boundary of the spot could not be applied owing to the lack of a database on the sum of umbra areas on the hemisphere. There are a number of works in which this umbra–penumbra boundary is discussed on the basis of direct observations (Jurčák 2011; Jurčák et al. 2015, 2017, 2018; Schmassmann et al. 2018; Lindner et al. 2020).

In this work, we have chosen the value of 1800 Mx cm^{-2} as the umbra boundary, which is quite close to the results of Jurčák (2011) and Jurčák et al. (2015, 2017, 2018). Hence, we obtain an average magnetic field of the umbra of 2000 Mx cm^{-2} (see Figure 3(b)).

As mentioned above, the temperature in stellar spots corresponds to the temperature of the sunspot umbra. Therefore, Figure 3(b) shows a diagram for the starspot umbra.

After having estimated the mean magnetic field B in sunspots and in starspots, let us estimate the scaling factors f_h, f_s, and f_r.

Assuming that the mechanism of solar and stellar flares is the same, this height should be approximately conserved. To determine the dependence of this height on spottedness, the factor $A^{1/2}$ is provided in Equation (9). It is easy to see that this multiplier gives too large values and reflects only the general trend. Hence, for areas 3×10^{-4}, 10^{-3}, 10^{-2}, and 10^{-1} of the solar hemisphere, we get the values of $A^{1/2}$ equal to 30, 50, 170, and 550 Mm, respectively. In the Sun, the estimated height of the energy release domain is 10–20 Mm (see, e.g., Sharykin et al. 2018, 2020; Zimovets et al. 2020). Therefore, for the Sun, we must take the parameter $f_h = 0.3$, while in superflaring stars we obtain $f_h = 0.1$.

Parameter f_s is a dimensionless scaling factor determining the share of the region occupied by the strongest magnetic field. This is actually the relative area of the umbra in a sunspot. We assume $f_s = 0.2$ (see Bludova et al. 2014).

When estimating f_s for the stars that produce superflares, we have to take into account that the spottedness A is expected to be large. In principle, a large spottedness can be achieved by increasing either the number or the size of spots. In the former case, however, the effect will be undetectable by observations based on the rotational modulation. Therefore, we have to assume that the observed stellar spottedness is determined by the relative area of the umbra of a single large stellar spot. In other words, for stars with superflares we have to assume $f_s = 1.0$.

Parameter f_r is part of the magnetic energy converted to radiation during a flare. When estimating f_r, one has to be more careful. Herbst et al. (2021), following Schrijver et al. (2012), who, in turn, followed Metcalf et al. (2005) and Schrijver et al. (2008), obtained $f_r = 0.01$–0.5 and based the width of the fitting strip on this estimate. Below, we will comment on this estimate in more detail.

Variations in the photospheric magnetic field in strong solar flares were investigated by Sudol & Harvey (2005), Petrie & Sudol (2010), and Maurya et al. (2012). Recently, Castellanos Durán et al. (2018) analyzed 77 solar flares and found out that most major flares (class above M1.6) were accompanied by abrupt and permanent variations in the photospheric magnetic field. They considered 38 X-class flares and 39 M-class flares. For each flare, they isolated an area in the corresponding active region where the field variation lasted as long as 15 minutes. The amplitude of the field variation ranged from the lower observational limit of about 10 G to about 450 G (two cases). The mean amplitude was 69 G. In the case of X-class flares, the variations used to be substantially larger than in the case of M-class flares. The authors insist that the above amplitude estimates are representative.

Livshits et al. (2015), Sharykin et al. (2018), Sharykin et al. (2020), Zimovets et al. (2020), and Artemyev et al. (2021) estimated the ratio of the free and total energy as 0.15–0.25. The results depend on the extrapolation method. However, only part of the free energy (from a few percent to dozens of percent) can be spent to create a flare. The volume of the flare

Table 1
Model Parameters

A, m.v.h.	B (Mx cm^{-2})	f_h	f_s	f_r	log E	H (km)
−3.5	800	0.3	0.2	0.1	30.659	9302
−3.0	900	0.3	0.2	0.1	31.511	16,543
−2.0	2000	0.1	1.0	0.1	33.926	17,438
−1.5	2000	0.1	1.0	0.1	34.676	31,009
−1.0	2000	0.1	1.0	0.1	35.426	55,144

occupies part of the active region only. During a flare, the energy can even grow somewhere inside the active region. The components of the photospheric magnetic field can grow stepwise during the flare (see, e.g., Petrie 2013; Sun et al. 2017, for the horizontal component; see Petrie & Sudol 2010, for the line-of-sight component). On the one hand, the buoyancy can transport the magnetic flux in the flaring region even during a flare; on the other hand, the flux can trigger the flare. There are flare models that take into account the energy income during the flare (e.g., Mogilevskii et al. 2005; Mogilevsky & Shilova 2006).

All these factors result in a difference of 2–3 orders of magnitude in the flaring power and thus account for C, M, and X flares. In principle, one can estimate f_r for individual flares or flares of particular types. Here, however, we are interested in the general link between the energy and spottedness. Therefore, we did not use the value of f_r in further calculations, since f_r and, to some extent, f_s cannot be reliably determined from observations and are not a general characteristic of the flare phenomenon. They determine the energy of each individual flare, leading to a huge scatter in the observed values.

A summary of the model parameters we adopted and the calculated values of energy E and flare height H are shown in Table 1 and Figure 4. A cloud of points from Maehara et al. (2015) is partially copied to the same figure for energies above 10^{30} erg and spottedness above 10^{-4} of the solar hemisphere. It can be seen that the values obtained by us generally agree with the observations. This figure is consistent with Figures 4 and 5 in Okamoto et al. (2021a) for Sun-like stars.

We conclude that the solar and stellar flares can be considered within the framework of a unique approach with specific governing parameters applied in the particular cases.

4. Discussion and Conclusions

Naturally, we (as well as all other authors we cite) assume that spots on the Sun and stars are of the same nature. In this case, the transformation of the rotational modulation into the area of the spot (or, more precisely, the umbra of the spot) using Equation (1) is quite natural and provides a basis for comparing the dependences of the number of flares on the spottedness. If we assume that sunspots and stars have different structures, then the very comparison of flare activity with spottedness loses its meaning and needs to be fundamentally revised.

We have demonstrated that the mechanisms of solar flares and stellar superflares are basically identical and the corresponding data can be described by Equation (9) with realistic parameters. A compact solar active region with the umbral area of the order of 0.1 of the solar hemisphere and the magnetic field $B = 2$ kG (which gives the magnetic field strength of about 100 G after averaging over the whole stellar surface) can produce a superflare with $E = (1 - 3) \times 10^{36}$ erg.

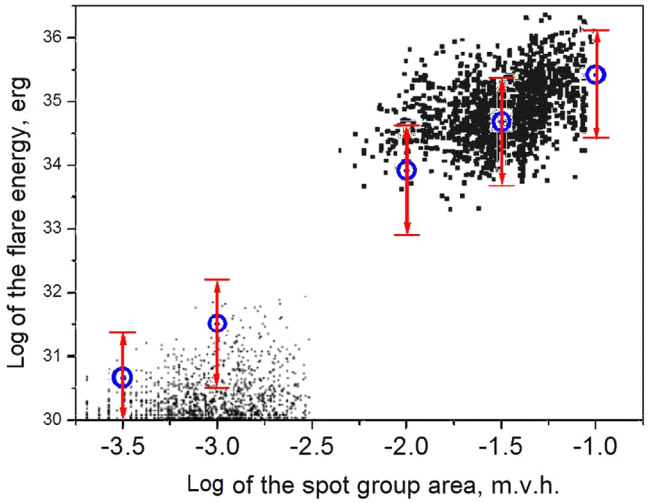

Figure 4. Flare energy vs. total spot group area. A cloud of points from Maehara et al. (2015) is partially copied to the same figure for energies above 10^{30} erg and spottedness above 10^{-4} of the solar hemisphere. Results of our calculations are shown by blue circles. The dispersion of energy values associated with the uncertainty of the parameter f_r (0.5–0.01) is shown in the figure with red arrows.

Thus, the flare generation mechanism can be the same on the Sun and stars. The main difference is that the spottedness on the Sun is no more than a few thousand m.h.v., while on the stars it reaches tenths of the area of the disk. As a result, the variation in the solar optical radiation is less than 0.1% (Fröhlich 2006, 2012), and on M dwarfs it reaches 10%. At the same time, flares on the Sun are 1–2 orders of magnitude less frequent than on these stars, and their energies do not exceed 3×10^{32} erg. The mean magnetic field in sunspots is lower by a factor of 2 than in giant spots associated with superflares. Accordingly, the magnetic flux on M dwarfs is 3 orders of magnitude higher than on the Sun.

The problem is why the solar dynamo produces magnetic fields associated with active regions of about 10^{-3} of the area of the solar hemisphere, i.e., by 2–3 orders of magnitude smaller than required to get a superflare (about $A = 0.1$ of the area of the stellar hemisphere). Note that earlier Katsova et al. (2021) admitted the possibility that superflares are governed by a physical mechanism basically different from the solar mechanisms. A comprehensive quantitative model that accumulates physical processes from dynamo action in the stellar interior up to the flare formation is far above contemporary theoretical abilities even for the Sun, not to mention other stars. Here we discuss some hints concerning this future theory that can be associated with superflares. Perhaps, to explain very high spottedness of superflaring stars, one may assume that the dynamo action domain on such stars is located just beneath the surface of the star rather than somewhere near the bottom of the convection zone, e.g., in the overshoot layer as is generally believed.

Indeed, helioseismology data indicate that the solar convection zone contains two layers of substantially differential rotation. One is the so-called overshoot layer near the bottom of the convection zone, while another is located near the solar surface. There are solar dynamo models with dynamo action concentrated in the upper layer of differential rotation (e.g., Brandenburg 2005); however, the models with deep location of the dynamo active region are more popular.

In order to produce an area with a strong magnetic field on the solar surface in the form of a sunspot, the dynamo-driven magnetic field has to propagate through a thick dynamo inactive layer. The magnetic field generated in the upper dynamo active layer has to propagate through a very thin layer only. Hence, it is reasonable to suggest that the spots produced in the latter case will be larger than those produced in the former case. Of course, this suggestion needs to be confirmed by a dynamo model that would include a more or less realistic description of the spot formation. There are various ideas concerning the particular mechanisms of formation of stellar spots (e.g., Parker 1975; Brandenburg et al. 2013; Jabbari et al. 2014; Getling et al. 2016), so that such confirmation requires an extensive modeling, which is, obviously, beyond the scope of this paper. Another helpful point is that the G dwarfs where very strong flares occur are fast rotators, and one can expect that dynamo drivers here are substantially stronger than in the Sun. It may also help to produce more magnetic energy than on the Sun. Further modification of the idea is to suppose that the distribution of the dynamo drivers on superflaring stars differs substantially from that on the Sun (e.g., the activity wave propagates mainly toward the surface rather than toward the equator), which produces even more magnetic energy (Kitchatinov & Olemskoy 2016; Katsova et al. 2018a, 2018b).

Note that the occurrence rate of weak flares (class C and even weaker subflares) is not related to the spottedness. These weak flares occur in the Sun almost every day, and their occurrence rate is almost independent of A (Figure 1).

We note that the points with error bars in Figure 4 do not exactly approximate the data for particular stellar flares. It looks possible to improve this fitting introducing additional parameters in the model; however, our intention is to show that the general shape of flare distribution can be fitted by a quite simple model and that various flares are related to compatible physical processes. We appreciate, however, that a further complication of the model may be interesting because it can be associated with the fact that morphology of stellar spots may be different from solar ones. In particular, we suppose here that the spots are more or less homogeneous. Supposing that very powerful solar flares are associated with sunspot groups that contain many smaller sunspots, which looks plausible according to available observations (McIntosh 1990; Toriumi & Wang 2019), one could obtain a lower estimate for the point with $A = -3.0$ in Figure 4.

To summarize our results, we can say that they are rather expected. Indeed, it looks plausible that larger spottedness gives more powerful stellar flares. Again, the very fact that the stellar activity cycles can be observed by contemporary observational methods means that there are stars with the spottedness substantially larger than observed in the Sun. We note, however, that the expected results must be supported by detailed argumentation, which is presented in this paper.

Thus, the problem of a sharp difference in energy between the solar and stellar flares does not require revision of the flare models. This difference is due to the fact that the efficiency of spot formation decreases with the age of the star and the increase of its rotation period. This issue was studied in detail from a theoretical point of view in Pipin (2021; see also numerous references therein). Observational data also confirm this dependence for a large number of stars (Tu et al. 2021). Here we concentrate attention mainly on G stars; however, M-dwarf data are obviously interesting in this respect; see Newton et al. (2017) and subsequent papers.

D.D.S. acknowledges support by BASIS fund No. 21-1-1-4-1. Authors acknowledge the financial support of the Ministry of Science and Higher Education of the Russian Federation, program 075-15-2020-780 (V.N.O., M.M.K) and 075-15-2022-284 (D.D.S.).

ORCID iDs

M. M. Katsova https://orcid.org/0000-0002-3367-7304
V. N. Obridko https://orcid.org/0000-0001-5100-806X
D. D. Sokoloff https://orcid.org/0000-0002-3441-0863
I. M. Livshits https://orcid.org/0000-0002-8390-013X

References

Artemyev, A., Zimovets, I., Sharykin, I., et al. 2021, ApJ, 923, 151
Aschwanden, M. J., Xu, Y., & Jing, J. 2014, ApJ, 797, 50
Aulanier, G., Démoulin, P., Schrijver, C. J., et al. 2013, A&A, 549, A66
Balona, L. A. 2015, MNRAS, 447, 2714
Belov, A., Garcia, H., Kurt, V., & Mavromichalaki, E. 2005, CosRe, 43, 165
Benz, A. O. 2008, LRSP, 5, 1
Benz, A. O., & Güdel, M. 2010, ARA&A, 48, 241
Berdyugina, S. V. 2005, LRSP, 2, 8
Bludova, N. G., Obridko, V. N., & Badalyan, O. G. 2014, SoPh, 289, 1013
Bondar', N. I., Katsova, M. M., & Shlyapnikov, A. A. 2021, Ge&Ae, 61, 1069
Borrero, J. M., & Ichimoto, K. 2011, LRSP, 8, 4
Brandenburg, A. 2005, ApJ, 625, 539
Brandenburg, A., Kleeorin, N., & Rogachevskii, I. 2013, ApJL, 776, L23
Brasseur, C. E., Osten, R. A., & Fleming, S. W. 2019, ApJ, 883, 88
Castellanos Durán, J. S., Kleint, L., & Calvo-Mozo, B. 2018, ApJ, 852, 25
Colombo, S., Petralia, A., & Micela, G. 2022, A&A, 661, A148
Emslie, A. G., Dennis, B. R., Shih, A. Y., et al. 2012, ApJ, 759, 71
Emslie, A. G., Kucharek, H., Dennis, B. R., et al. 2004, JGRA, 109, A10104
Fernández, M., Stelzer, B., Henden, A., et al. 2004, A&A, 427, 263
Fröhlich, C. 2006, SSRv, 125, 53
Fröhlich, C. 2012, SGeo, 33, 453
García-Alvarez, D., Foing, B. H., Montes, D., et al. 2003, A&A, 397, 285
Gershberg, R. E. 2005, Solar-Type Activity in Main-Sequence Stars (Berlin: Springer)
Gershberg, R. E., Mogilevskii, E. I., & Obridko, V. N. 1987, KFNT, 3, 3
Gershberg, R. E., & Pikel'ner, S. B. 1972, CoASP, 4, 113
Getling, A. V., Ishikawa, R., & Buchnev, A. A. 2016, SoPh, 291, 371
Herbst, K., Papaioannou, A., Airapetian, V. S., & Atri, D. 2021, ApJ, 907, 89
Jabbari, S., Brandenburg, A., Losada, I. R., Kleeorin, N., & Rogachevskii, I. 2014, A&A, 568, A112
Jackman, J. A. G., Wheatley, P. J., Pugh, C. E., et al. 2018, MNRAS, 477, 4655
Jurčák, J. 2011, A&A, 531, A118
Jurčák, J., Bello González, N., Schlichenmaier, R., & Rezaei, R. 2015, A&A, 580, L1
Jurčák, J., Bello González, N., Schlichenmaier, R., & Rezaei, R. 2017, A&A, 597, A60
Jurčák, J., Rezaei, R., González, N. B., Schlichenmaier, R., & Vomlel, J. 2018, A&A, 611, L4
Kashapova, L. K., Broomhall, A.-M., Larionova, A. I., Kupriyanova, E. G., & Motyk, I. D. 2021, MNRAS, 502, 3922
Katsova, M. M., Kitchatinov, L. L., Livshits, M. A., et al. 2018a, ARep, 62, 72
Katsova, M. M., Kitchatinov, L. L., Moss, D., Oláh, K., & Sokoloff, D. D. 2018b, ARep, 513, 62
Katsova, M. M., & Livshits, M. A. 2015, SoPh, 290, 3663
Katsova, M. M., & Nizamov, B. A. 2018, Ge&Ae, 58, 899
Katsova, M. M., Obridko, V. N., Sokoloff, D. D., & Livshits, I. M. 2021, Ge&Ae, 61, 1063
Keppens, R., & Martinez Pillet, V. 1996, A&A, 316, 229
Kitchatinov, L. L., & Olemskoy, S. V. 2016, MNRAS, 459, 4353
Koller, F., Leitzinger, M., Temmer, M., et al. 2021, A&A, 646, A34
Kretzschmar, M. 2011, A&A, 530, A84
Lindner, P., Schlichenmaier, R., & Bello González, N. 2020, A&A, 638, A25
Livshits, M. A., Rudenko, G. V., Katsova, M. M., & Myshyakov, I. I. 2015, AdSpR, 55, 920

Maehara, H., Shibayama, T., Notsu, S., et al. 2012, Natur, 485, 478
Maehara, H., Shibayama, T., Notsu, Y., et al. 2015, Ep&S, 67, 59
Martiol, E., Hébrard, G., Correia, A. C. M., Laskar, J., & Lecavelier des Etangs, A. 2021, A&A, 649, 19
Maurya, R. A., Vemareddy, P., & Ambastha, A. 2012, ApJ, 747, 134
McIntosh, P. S. 1990, SoPh, 125, 251
Metcalf, T. R., Leka, K. D., & Mickey, D. L. 2005, ApJL, 623, L53
Mogilevskii, E. I., Obridko, V. N., & Shilova, N. S. 2005, A&AT, 24, 25
Mogilevsky, E. I., & Shilova, N. S. 2006, Ge&Ae, 46, 303
Namekata, K., Maehara, H., Notsu, Y., et al. 2019, ApJ, 871, 187
Newton, E. R., Irwin, J., Charbonneau, D., et al. 2017, ApJ, 834, 85
Notsu, Y., Shibayama, T., Maehara, H., et al. 2013, ApJ, 771, 127
Obridko, V. N., & Shelting, B. D. 2018, RNAAS, 2, 40
Okamoto, S., Notsu, Y., Maehara, H., et al. 2021a, ApJ, 906, 72
Okamoto, S., Notsu, Y., Maehara, H., et al. 2021b, Statistical Properties of Superflares on Solar-type Stars: Results Using All of the Kepler Primary Mission Data v1, Zenodo, doi:10.5281/zenodo.4563244
Parker, E. N. 1963, ApJS, 8, 177
Parker, E. N. 1975, ApJ, 198, 205
Petrie, G. J. D. 2013, SoPh, 287, 415
Petrie, G. J. D., & Sudol, J. J. 2010, ApJ, 724, 1218
Pipin, V. V. 2021, MNRAS, 502, 2565
Priest, E. R., & Forbes, T. G. 2002, A&ARv, 10, 313
Sammis, I., Tang, F., & Zirin, H. 2000, ApJ, 540, 583
Schmassmann, M., Schlichenmaier, R., & Bello González, N. 2018, A&A, 620, A104
Schmitt, J. H. M. M., Ioannidis, P., Robrade, J., Czesla, S., & C, S. P. 2019, A&A, 628, 9
Schrijver, C. J., Beer, J., Baltensperger, U., et al. 2012, JGRA, 117, A08103
Schrijver, C. J., DeRosa, M. L., Metcalf, T., et al. 2008, ApJ, 675, 1637
Sharykin, I. N., Zimovets, I. V., & Myshyakov, I. I. 2020, ApJ, 893, 159
Sharykin, I. N., Zimovets, I. V., Myshyakov, I. I., & Meshalkina, N. S. 2018, ApJ, 864, 156
Shibayama, T., Maehara, H., Notsu, S., et al. 2013, ApJS, 209, 5
Solanki, S. K., Inhester, B., & Schüssler, M. 2006, RPPh, 69, 563
Somov, B. V. 2013, Plasma Astrophysics, Part II, Vol. 392 (New York: Springer)
Sudol, J. J., & Harvey, J. W. 2005, ApJ, 635, 647
Sun, X., Hoeksema, J. T., Liu, Y., Kazachenko, M., & Chen, R. 2017, ApJ, 839, 67
Toriumi, S., & Wang, H. 2019, LRSP, 16, 3
Tu, Z.-L., Yang, M., Wang, H. F., & Wang, F. Y. 2021, ApJS, 253, 35
Vilmer, N. 2012, RSPTA, 370, 3241
Zimovets, I. V., Sharykin, I. N., & Gan, W. Q. 2020, ApJ, 891, 138